THE ASTROPHYSICAL JOURNAL, 435:L67–L70, 1994 November 1

THE PURSUIT OF HEAVY ELEMENTS IN THE HgMn-TYPE STAR χ LUPI: OBSERVATIONS WITH THE GHRS IN THE COSTAR ERA[1]

GLENN M. WAHLGREN,[2,3] TOMAS BRAGE,[3,4] RONALD L. GILLILAND,[5] SVENERIC G. JOHANSSON,[6,7]
DAVID S. LECKRONE,[3,8] DON J. LINDLER[3,9] AND ULF LITZÉN[6]
Received 1994 May 13; accepted 1994 August 11

ABSTRACT

Observations of the ultra–sharp-lined HgMn star χ Lupi made with the Goddard High Resolution Spectrograph after the *Hubble Space Telescope* First Servicing Mission display the effect of COSTAR corrective optics upon the spectral resolution of several observing modes. The resolution is restored to levels expected in the absence of the telescope spherical aberration for all observations made through the GHRS Large Science Aperture (LSA). The Small Science Aperture (SSA) spectra are nearly identical in resolution to the pre-COSTAR values while benefiting from higher throughput. The line spread function for the LSA relative to the SSA shows little wavelength dependence and reflects a Gaussian profile ~20%–30% broader than for SSA spectra. Absorption features containing components of As II and Bi II represent upper limit enhancements of 2.9 and 2.1 dex for As II and Bi II, respectively, relative to meteoritic abundance determinations.

Subject headings: stars: abundances — stars: individual (χ Lupi) — stars: peculiar — ultraviolet: stars

1. INTRODUCTION

The flawless installation of the Corrective Optics Space Telescope Axial Replacement instrument (COSTAR) by the STS-61 astronauts during the *Hubble Space Telescope* (*HST*) First Servicing Mission has essentially restored the spectral resolution capabilities of the Goddard High Resolution Spectrograph (GHRS) to specifications established before the realization of the telescope spherical aberration. The enhancement of spectral resolution is particularly apparent in spectra obtained through the instrument's Large Science Aperture (LSA). As a result of the tightening of the GHRS point spread function by the COSTAR optics, the throughput has been increased by nearly a factor of 2 for the Small Science Aperture (SSA) while remaining with 10% of the pre-COSTAR levels for the LSA.

An observing program was created as part of the post-COSTAR installation Servicing Mission Orbital Verification (SMOV) testing program to characterize the spectral resolution and wavelength dependence of the GHRS line-spread function (LSF) in the COSTAR environment. By nature of its ultra–sharp-lined spectrum, resulting from an extremely low rotational velocity ($v \sin i = 1$ km s^{-1}) and atmospheric turbulence ($V_{\rm turb} = 0$ km s^{-1}), the HgMn-type star χ Lupi is an excellent target for this purpose. This fortuitous test opportunity has allowed us to obtain spectra that can be used to search for atomic transitions from heavy elements that have not been identified at lower spectral resolutions or in other spectral regions. In this *Letter* we discuss the detection and abundance determinations for singly ionized arsenic and bismuth.

2. OBSERVATIONAL DATA

Observing program SMOV 4808 was executed on 1994 February 17, obtaining high-quality spectra with both the LSA and SSA. Data were collected with the echelle-B and first-order gratings (G160M, G200M, G270M) at central wavelengths of 1910 and 2680 Å, and with the G160M grating alone at a central wavelength of 1360 Å. The GHRS side 1 was not operational at the time of the observations, thereby precluding echelle-A mode data for the shortest central wavelength. As a result of a GHRS grating carrousel failure to lock, the observation scheduled with the G270M grating at 2682 Å through the LSA was not obtained. A typical reduced spectrum possesses a signal-to-noise (S/N) ratio of ~100:1 at the continuum level, and an absolute wavelength scale calibrated to within ±0.5 diode. The final absolute wavelength scales were established to within ±0.001 Å from iron-group element Fourier Transform Spectrometer (FTS) data obtained with the Lund VUV-FTS. Data pertinent to the spectra collected are presented in Table 1. A program similar to SMOV 4808, but with a central wavelength setting of 1860 Å instead of 1910 Å, was executed twice in the pre-COSTAR era (proposal 3372). Thus, useful comparisons can be made at similar wavelengths between pre- and post-COSTAR installation data sets.

3. SPECTRAL RESOLUTION

For its first 3 years of operation the GHRS has provided UV spectral resolution and sensitivity unsurpassed by previous space-based instruments. As a result of *HST* spherical aberration, its highest spectral resolutions ($R = \lambda/\Delta\lambda = 80{,}000$–95,000) were attainable by using the echelle grating in conjunction with the SSA. With the introduction of COSTAR optics the highest resolution capabilities are extended to the LSA with only a modest degradation in resolution. Figure 1 compares the GHRS resolution capabilities for three observing

[1] Based on observations with the NASA/ESA *Hubble Space Telescope*, obtained at the Space Telescope Science Institute, which is operated by the Association of Universities for Research in Astronomy, Inc., under NASA contract NAS5-26555.

[2] Astronomy Programs, Computer Sciences Corporation and GHRS Science Team.
[3] Code 681, Goddard Space Flight Center, Greenbelt, MD 20771.
[4] National Research Council Resident Research Associate.
[5] Space Telescope Science Institute, 3700 San Martin Drive, Baltimore, MD 21218.
[6] Department of Physics, University of Lund, Sölvegatan 14, S-223 62 Lund, Sweden.
[7] Lund Observatory, Lund University, Box 43, S-22100 Lund, Sweden.
[8] Laboratory for Astronomy and Solar Physics, NASA/GSFC.
[9] Advanced Computer Concepts, Inc.

TABLE 1

PARAMETERS OF THE χ LUPI GHRS/COSTAR OBSERVATIONS

OBSERVATION ID	DATE[a] (JD - 2,440,000)	APERTURE/ GRATING[b]	SPECTRAL COVERAGE (Å)	EXPOSURE TIME[c] (s)	AVERAGE COUNT RATE[d] BACKGROUND	AVERAGE COUNT RATE[d] STELLAR
Z28H0108	9401.185	LSA/Ech-B(21)	2674.1-2688.4	323.14	4.42	176.41
Z28H0109	9401.191	LSA/Ech-B(29)	1904.7-1915.7	1292.54	3.13	23.57
Z28H010B	9401.244	LSA/G270M	2662.1-2709.9	107.71	1.19	642.97
Z28H010D	9401.247	LSA/G200M	1878.7-1919.9	323.14	0.42	144.88
Z28H010F	9401.254	LSA/G160M	1882.8-1917.8	430.85	0.23	91.67
Z28H010G	9401.261	LSA/G160M	1341.3-1378.3	430.85	0.38	123.78
Z28H010L	9401.325	SSA/Ech-B(21)	2674.1-2688.4	646.27	2.62	108.41
Z28H010M	9401.335	SSA/Ech-B(29)	1904.7-1915.7	2585.09	1.59	13.54
Z28H010Q	9401.443	SSA/G200M	1878.9-1920.1	646.27	0.26	84.84
Z28H010S	9401.454	SSA/G160M	1882.9-1917.8	861.70	0.12	47.72
Z28H010T	9401.466	SSA/G160M	1341.4-1378.3	861.70	0.18	54.48

[a] Date corresponds to the Unique Data Log readout start time, following the last subexposure.

[b] Echelle order number within parentheses.

[c] Exposure time for all six data bins, four science and two background. The exposure time for science data is 0.94117 times the listed value, the remainder being spent on background data collection. Step patterns of 7 and 5 were used for the echelle and first-order gratings, respectively.

[d] Count rate, in counts^{-1} s^{-1} per sample. A single sample corresponds to one diode of a given data bin. An average S/N for an observation may be estimated from [(exposure time × 0.94117/4) × (stellar − background)]$^{1/2}$. Maximum S/N in the continuum will be higher than the average value.

modes, both prior to and after COSTAR installation. It is clear that an enhancement in spectral resolution is realized for the LSA observations, while the SSA echelle resolution is essentially unchanged.

The acquisition of LSA and SSA spectra that contain similar wavelengths allows us to apply deconvolution algorithms to extract relative LSFs as a function of wavelength and grating mode. Pre-COSTAR, this differential LSF (see Gilliland et al. 1992) was characterized by a Gaussian core slightly broader than the instrumental resolution provided by SSA observations, and in addition had broad wings arising from the spherical aberration halo of the *HST* point spread function. The LSF of the LSA may be approximated as a convolution of the LSA to SSA differential LSF onto the SSA LSF (a Gaussian of FWHM 3.7 pixels). Post-COSTAR, the differential LSF is characterized by a Gaussian core significantly narrower than the instrumental resolution of the SSA, and correction for the *HST* spherical aberration has effectively removed the broad wings. The full LSA LSF is 20%–30% broader than that provided by the SSA and is evident in the Figure 1 comparisons. From this data set no trends with wavelength or spectral element are considered significant (Gilliland 1994).

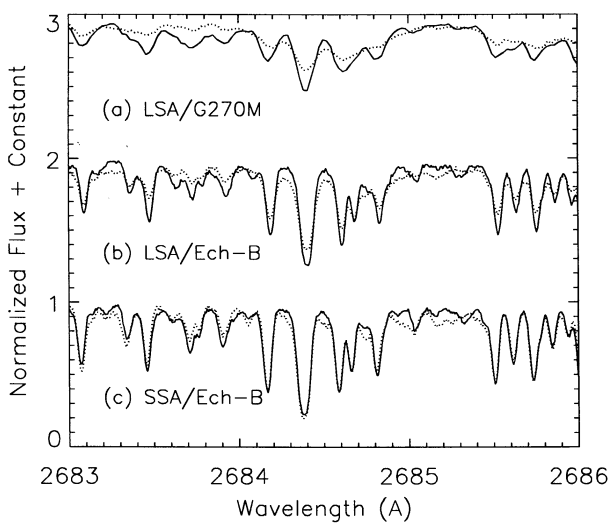

FIG. 1.—Comparison of spectra obtained before (*dotted*) and after (*solid*) COSTAR installation for three GHRS observing modes. Differences in the compared spectra due to resolution effects are evident by the depth variations of prominent lines, while small-scale discrepancies such as those in the SSA/Ech-B spectrum are the result of different binary orbital phases.

4. ABUNDANCE ANALYSIS

χ Lupi (B9.5p + A2 V; $V = 3.95$) is one of the coolest members of the nonmagnetic, HgMn class of chemically peculiar (CP) stars. Its atmospheric parameters and elemental abundances have been determined from high-resolution optical region spectra, most recently by Wahlgren, Adelman, & Robinson (WAR 1994). However, at optical wavelengths a less than favorable light ratio for study of the primary star and a dearth of strong, low-excitation transitions for ions of many of the heaviest elements has necessitated exploration of the ultraviolet domain.

We have detected absorption features in first-order spectra which contain contributions from As II and Bi II. An abundance of [As I/H] = +1.8 had already been determined for χ Lupi from the unblended 1937.594 Å transition (Leckrone et al. 1993). No abundance value has previously been determined for bismuth in this star, and to our knowledge the only prior detection of Bi II in a CP star is that for HR 7775 (Jacobs & Dworetsky 1982), for which an enhancement of [Bi II/H] = +6.0 was determined. For both arsenic and bismuth, the comparison to solar system abundances refers to meteoritic abundance determinations (Anders & Grevesse 1989), as no lines from either element have been detected in the solar spectrum.

We employ a synthetic spectrum technique to derive abundances, in a manner similar to that discussed by Leckrone et al. (1993) and WAR. The synthetic spectra were generated for both components of the binary using the SYNTHE code

(Kurucz & Avrett 1981) and the atmospheric model parameters of WAR. For comparison with an observation, the computed normalized synthetic component spectra were offset in wavelength by an amount determined from the observation start time and the orbital ephemeris of Dworetsky (1972), weighted by the wavelength-dependent luminosity ratio, coadded, and convolved with an LSF (R = 18,640 and 29,000 for observations Z28H010T and Z28H010S, respectively, based upon a Gaussian point-spread function) appropriate to the wavelength and grating mode. Luminosity ratios, (L_A/L_B), of 6.63 and 11.15 were interpolated from the data presented by Leckrone et al. (1994), for the observations centered near 1900 and 1360 Å, respectively. The atomic line data, excluding that for the arsenic and bismuth lines, are from the compilations of Kurucz (1991). Wavelengths, oscillator strengths, and hyperfine structure (HFS) for the As II and Bi II transitions were obtained by combining laboratory measurements with theoretical multiconfiguration calculations. The details and results of the calculations, i.e., oscillator strengths and HFS parameters, will be published elsewhere.

The strongest transition of Bi II in the observed intervals is the $6p^2\,{}^3P_2$–$6p7s\,{}^3P_1$ transition at 1902.3 Å. Its nine hyperfine components have been studied by Bouazza & Bauche (1988), but until now no accurate absolute wavelengths or oscillator strengths were available. The wavelengths have now been measured with the FTS at Lund to an uncertainty of less than 1 mÅ. Oscillator strengths and HFS were obtained from an Extended Optimal Level (EOL) calculation using the GRASP2 program (Parpia & Grant 1991). Table 2 presents the experimental and theoretical values for the separations ($\Delta\lambda$) of the HFS components, each defined by the total angular momentum, F, of the lower and upper levels of the transition. There is good agreement between theory and experiment for the hyperfine splitting of the Bi II line which implies that HFS data from extended theoretical calculations can be used in synthetic spectra when no experimental data are available. Table 2 also presents the peak intensity, I, of the laboratory lines as a measure of the relative intensities. To facilitate the comparison of the measured line intensities to the theoretically derived gf-values we have normalized the intensity scale to match the calculated gf-values. In general, the agreement is very good, but a small discrepancy occurs for the 7/2–9/2 and 13/2–11/2 components, which are not fully resolved in the FTS spectrum.

The abundance determination of Bi II based on the line λ1902.3 is problematic due to uncertainties in blending contributors. We have included in the calculation a representative

TABLE 2

HYPERFINE STRUCTURE IN Bi II λ1902.3

		Experiment			Theory	
F_l	F_u	I	λ (Å)	Δλ (mÅ)	Δλ (mÅ)	GF
4.5	5.5	14	1902.265	...	...	0.013
5.5	5.5	59	1902.288	23	23	0.059
6.5	5.5	159	1902.314	26	27	0.168
3.5	4.5	43	1902.325	11	-3	0.037
4.5	4.5	75	1902.343	18	19	0.078
5.5	4.5	85	1902.365	22	23	0.085
2.5	3.5	72	1902.374	9	-3	0.072
3.5	3.5	59	1902.388	15	15	0.059
4.5	3.5	30	1902.407	19	19	0.029

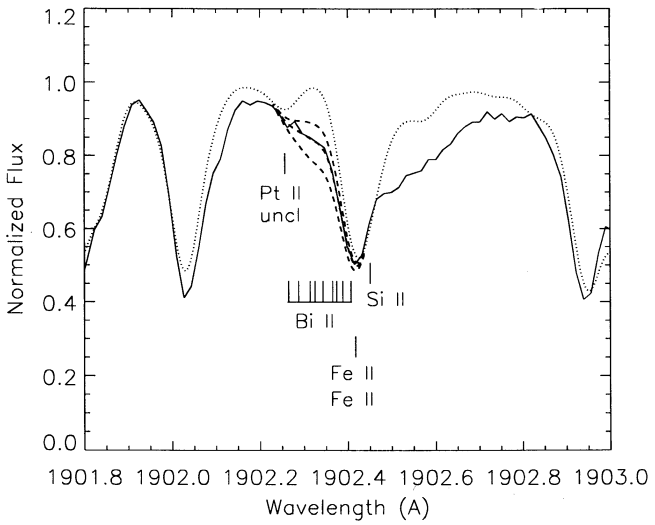

FIG. 2.—Detection of Bi II. The SSA/G160M observation in the vicinity of Bi II λ1902.3 (*solid curve*) is compared to theoretical spectra computed with a solar system bismuth abundance (*dotted curve*) and enhancements [Bi II/H] = +1.9, 2.1, and 2.3 (*dashed curve*). The locations of the Bi II hyperfine components are labeled along with prominent blending components. The abundance of (Bi II/H) = +2.8, [Bi II/H] = +2.1, provides the best fit and represents an upper limit for this ion as a result of the uncertain characterization of the Si II line profile.

Pt II line at the position of the unclassified Pt λ1902.26 line (Sansonetti et al. 1992). The Si II λ1902.4 photoionization resonance, a result of an autoionizing upper level, has been modeled in our calculation by a Voigt profile with gf = 0.2. Its width has been measured to be $\Delta\lambda$ = 0.25 Å (Artru & Lanz 1987) from photographic plate data, but its exact Fano profile is undetermined. If its wavelength and width are accurate then it likely contributes to the opacity at the location of the Bi II feature, reducing the derived Bi II abundance. The best fit to the observed spectrum (Fig. 2) occurs for the abundance (Bi II/H) = +2.8 (on the scale log H = 12.00), or [Bi II/H] = +2.1, and is considered an upper limit. Thus, the abundance enhancement of Bi II is considerably lower than that for Pt II, Au II, Hg II, and Tl II in χ Lupi and the Bi II enhancement reported for HR 7775.

Three As II lines in the vicinity of λ1375 have been studied, UV multiplet (1) λλ1373.650, 1375.783 and UV (4) λ1375.07, for which center of gravity wavelengths with an uncertainty of 3–8 mÅ have been published by Li & Andrew (1971). For the calculation of oscillator strengths and HFS it is sufficient to use a semirelativistic method, based on the multiconfiguration Hartree-Fock technique, augmented by a Breit-Pauli configuration interaction (CI) calculation (Froese-Fischer 1991; Brage & Froese-Fischer 1993). An uncertainty of ~10% in oscillator strength is estimated for the $4p^2\,{}^1D_2$–$4p5s\,{}^1P_1$ transition at 1375.07 Å. The wavelengths of the hyperfine components in this line have been obtained by combining the calculated HFS and the laboratory wavelength.

The UV multiplet (4) line λ1375.07 is the intrinsically strongest of the three lines, having a calculated gf = 0.96, and serves as our primary As II abundance indicator. Its HFS components have been included in our line list but only extend over a 3 mÅ range and therefore exhibit no observable line broadening in the first-order grating spectrum. To derive an accurate abundance from this line it was necessary to decrease the f-value for Ti II λ1374.980 in order that the calculation not

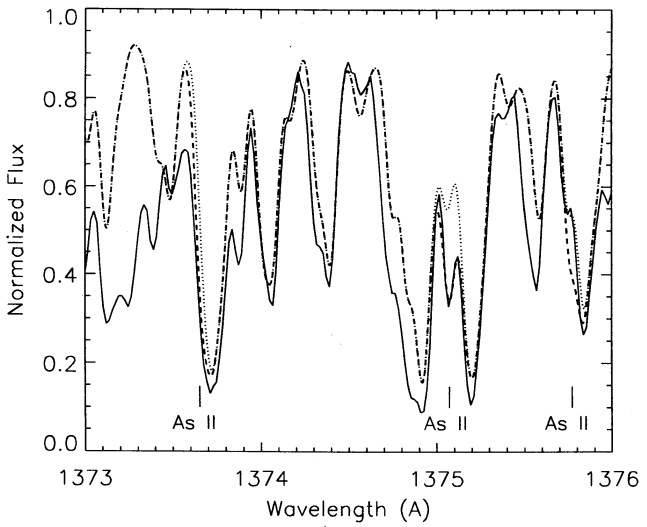

FIG. 3.—Detection of As II in the 1373–1376 Å region. The positions of three As II lines are labeled in the χ Lupi spectrum. The observed spectrum (*solid curve*) is compared against synthetic spectra (*dashed curve*) for the abundances [As II/H] = 0.0 and +2.9. The poor fit displayed for As II λ1375.783 is most likely due to a poor oscillator strength for Ti II λ1375.741.

violate the bounds of the observation; otherwise, its opacity contribution to the As II line translates into an abundance variation of $\sim$0.2 dex. Laboratory Ti II line strengths (Huldt, Johansson, & Litzen 1982) support weakening the Ti II oscillator strength. The poor fit in Figure 3 for the weaker As II λ1375.783 ($gf = 0.0007$) line at the enhanced abundance is due to an erroneously high f-value either for the line itself or Ti II λ1375.741, which has not been altered in our calculations. The As II λ1373.650 line ($gf = 0.007$) does not suffer from problems associated with Ti blending. The observation near the As II λ1375.07 line is well fitted by the abundance (As II/H) = +5.23, or [As II/H] = +2.9, which is 1.1 dex greater than the abundance from As I λ1937.594. Although we have considered all known blending components with As II λ1375.07, in particular by the addition of Zr III λ1375.130 (calculated $gf = 0.0001$), the derived abundance for As II must be considered an upper limit.

This work was supported by NASA grant NAS5-30523. Members of the GHRS team gratefully acknowledge the successful efforts of the STS-61 astronauts in servicing the *HST* and restoring GHRS capabilities. We also thank the referee, R. Kurucz, for insightful comments.

REFERENCES

Anders, E., & Grevesse, N. 1989, Geochim. Cosmochim. Acta, 53, 197
Artru, M.-C., & Lanz, T. 1987, A&A, 182, 273
Bouzza, S., & Bauche, J. 1988, Z. Phys. D, 10, 1
Brage, T., & Froese-Fischer, C. 1993, Phys. Scripta, T47, 18
Dworetsky, M. M. 1972, PASP, 84, 254
Froese-Fischer, C. 1991, Comput. Phys. Commun. 64, 369
Gilliland, R. L. 1994, GHRS Instrument Science Rep., No. 63 (Baltimore: STScI)
Gilliland, R. L., Morris, S. L., Weyman, R. J., Ebbets, D. C., & Lindler, D. J. 1992, PASP, 104, 367
Huldt, S., Johansson, S., & Litzén, U. 1982, Phys. Scripta, 25, 401
Jacobs, J. M., & Dworetsky, M. M. 1982, Nature, 299, 535
Kurucz, R. L. 1991, in Stellar Atmospheres: Beyond Classical Methods, ed. L. Crivellari, I. Hubeny, & D. G. Hummer (Dordrecht: Kluwer), 441
Kurucz, R. L., & Avrett, E. H. 1981, Smithsonian Astrophys. Obs. Spec. Rept., No. 391
Leckrone, D. S., Johansson, S., Wahlgren, G. M., & Adelman, S. J. 1993, Phys. Scripta, T47, 149
Leckrone, D. S., et al. 1994, in preparation
Li, H., & Andrew, K. L. 1971, J. Opt. Soc. Am., 61, 96
Parpia, F. A., & Grant, I. P. 1991, J. Phys., Suppl. II, C1
Sansonetti, J. E., Reader, J., Sansonetti, C. J., & Acquista, N. 1992, J. Res. Nat. Inst. Standards Tech., 97, 1
Wahlgren, G. M., Adelman, S. J., & Robinson, R. D. 1994, ApJ, 434, 349